



UNIVERSITY OF LEEDS

This is a repository copy of *Electrostatic-Driven Activity, Loading, Dynamics, and Stability of a Redox Enzyme on Functionalized-Gold Electrodes for Bioelectrocatalysis*.

White Rose Research Online URL for this paper:
<http://eprints.whiterose.ac.uk/140711/>

Version: Accepted Version

Article:

Hitaishi, VP, Mazurenko, I orcid.org/0000-0003-2563-3130, Harb, M et al. (8 more authors) (2018) *Electrostatic-Driven Activity, Loading, Dynamics, and Stability of a Redox Enzyme on Functionalized-Gold Electrodes for Bioelectrocatalysis*. *ACS Catalysis*, 8 (12). pp. 12004-12014. ISSN 2155-5435

<https://doi.org/10.1021/acscatal.8b03443>

© 2018 American Chemical Society. This is an author produced version of a paper published in *ACS Catalysis*. Uploaded in accordance with the publisher's self-archiving policy.

Reuse

Items deposited in White Rose Research Online are protected by copyright, with all rights reserved unless indicated otherwise. They may be downloaded and/or printed for private study, or other acts as permitted by national copyright laws. The publisher or other rights holders may allow further reproduction and re-use of the full text version. This is indicated by the licence information on the White Rose Research Online record for the item.

Takedown

If you consider content in White Rose Research Online to be in breach of UK law, please notify us by emailing eprints@whiterose.ac.uk including the URL of the record and the reason for the withdrawal request.



eprints@whiterose.ac.uk
<https://eprints.whiterose.ac.uk/>

1 **Electrostatic-driven activity, loading, dynamics and stability of a redox**
2 **enzyme on functionalized-gold electrodes for bioelectrocatalysis**

3 Vivek Pratap Hitaishi,^[a] Ievgen Mazurenko,^[b] Malek Harb,^[a] Romain Clément,^[a] Marion
4 Taris,^[c] Sabine Castano,^[c] David Duché,^[d] Sophie Lecomte,^[c] Marianne Ilbert,^[a] Anne de
5 Poulpiquet,^[a] Elisabeth Lojou*^[a]

6
7 ^[a]Aix-Marseille Univ, CNRS, BIP, UMR 7281, 31 Chemin Aiguier, 13009 Marseille, France

8 ^[b] School of Biomedical Sciences, University of Leeds, LS2 9JT Leeds, UK

9 ^[c] Institute for Chemistry and Biology of Membrane and Nano-objects, Allée Geoffroy St Hilaire, 33600
10 Pessac, France

11 ^[d] Aix Marseille Université, CNRS, Université de Toulon, IM2NP UMR 7334, 13397

12 Marseille, France

13

14 **ABSTRACT: Oxygen reduction reaction is the limiting step in fuel cells, and many**
15 **works are in progress to find efficient cathode catalysts. Among them, bilirubin oxidases**
16 **are copper-based enzymes that reduce oxygen into water with low overpotentials. The**
17 **factors that ensure electrocatalytic efficiency of the enzyme in the immobilized state are**
18 **not well understood, however. In this work, we use a multiple methodological approach**
19 **on a wide range of pH for protein adsorption and for electrocatalysis, to demonstrate**
20 **the effect of electrostatic interactions on the electrical wiring, dynamics and stability of a**
21 **bilirubin oxidase adsorbed on self-assembled-monolayers on gold. We show on one hand**
22 **that the global charge of the enzyme controls the loading on the interface, and that the**
23 **specific activity of the immobilized enzyme decreases with the enzyme coverage. On the**
24 **other hand, we show that the dipole moment of the protein and the charge in the vicinity**
25 **of the Cu site acting as the entry point of electrons, drive the enzyme orientation. In case**
26 **of weak electrostatic interactions, we demonstrate that local pH variation affects the**

27 **electron transfer rate as a result of protein mobility on the surface. On the contrary,**
28 **stronger electrostatic interactions destabilize the protein structure and affect the**
29 **stability of the catalytic signal. These data illustrate the interplay between immobilized**
30 **protein dynamics and local environment that control the efficiency of bioelectrocatalysis.**

31 KEYWORDS: Enzymes; Catalysis; Self-Assembled-Monolayers; Electrochemistry;
32 Ellipsometry; Surface Plasmon Resonance; PMIRRAS.

33

34 INTRODUCTION

35 In an upcoming rising sustainable economy, fuel cells may play a role in the energy
36 production. One of their limitations is the low efficiency of the oxygen reduction reaction
37 (ORR), imposing the research of a catalyst combining high performance, stability and
38 renewability¹⁻⁴. Redox enzymes are such catalysts that efficiently operate in microorganisms
39 to convert substrates. Among them, bilirubin oxidase (BOD), which belongs to the multi
40 copper oxidase family, is one of the most considered alternative to platinum for oxygen
41 reduction in enzymatic fuel cells⁵⁻⁶. The global catalytic cycle performed by this enzyme
42 immobilized on electrochemical interfaces is now well established^{5,7}. It involves four copper
43 centers, the CuT1 being the one which accepts the electrons from the reductant, and will
44 therefore be the entry point of electrons from the electrode. Although enhanced catalytic
45 performance has been achieved by entrapment of BOD in various carbon and metal
46 nanomaterials⁸⁻¹¹, BOD-based bioelectrodes still suffer from low stability, precluding
47 industrial use of the related biodevices. As an illustration, recent works in our laboratory
48 showed that the half life of a BOD-based bioelectrode incorporated in carbon felts was
49 restricted to one week at room temperature¹². Furthermore, for direct wiring of a redox
50 enzyme on a conductive support, it is mandatory to allow an electron tunneling between the
51 enzyme active site and the electrode, and to permit substrate access¹³⁻¹⁷. By varying the pH of

52 BOD adsorption on a carbon nanotube (CNT) network, Mazurenko et al. demonstrated that
53 electrostatic interactions were driving the adsorption process in an orientation favoring either
54 this direct wiring (direct electron transfer, DET), or a connection via a diffusing redox
55 mediator (MET) ¹⁵. However, even after having defined the surface chemistry required for an
56 efficient direct wiring, it was calculated that less than 10 % of the loaded enzymes were
57 effectively participating to the catalysis ¹². Similar low percentage of electroactive enzymes
58 was reported recently for laccase, another multicopper protein, on amorphous carbon nitride
59 ¹⁸.

60 Understanding the factors that affect this low catalytic efficiency is thus required. While
61 porous electrodes may enhance the loading of enzymes, planar electrodes are much more
62 appropriate for the fundamental studies of enzyme immobilization ^{14, 19-22}. In particular, planar
63 gold surfaces are mostly used in methods allowing to study loading of enzymes on solid
64 supports (surface plasmon resonance (SPR), quartz crystal microbalance (QCM)), or enzyme
65 conformation in the immobilized state (Surface-Enhanced Infrared Absorption (SEIRA),
66 Surface-Enhanced Raman Spectroscopy (SERS), Polarization Modulation Infrared Reflection
67 Adsorption Spectroscopy (PMIRRAS)) ^{14, 23-24}. Coupling these methods to electrochemistry is
68 utmost crucial to be able to correlate electroenzymatic activity to enzyme amount and
69 conformation, and to study the dynamics of the immobilized enzyme, with the ultimate goal
70 of proposing bioelectrode rationalization ²⁵. Self-assembled-monolayers (SAMs) appear as
71 fine tools allowing to easily tune and control the chemistry and charge of a planar gold
72 electrochemical interface, while being rid of the complex surface chemistry and porosity of
73 nanomaterials, which could influence the electrochemical response. Varying the pH may offer
74 the additional advantage of changing the interactions between the surface and the enzyme by
75 affecting both components in a controllable manner. However, the dynamics of the
76 immobilized enzyme upon local pH change in the course of electrocatalysis has been rarely

77 investigated. One can cite the study by Jin et al. who investigated the pH-dependent
78 interfacial electron transfer of cytochrome c electrostatically bound to a SAM ²⁶.
79 In this work we bring new insight towards the comprehensive enzyme immobilization by the
80 unprecedented coupling of electrochemistry to SPR, PMIRRAS and ellipsometry.
81 Myrothecium verrucaria BOD (Mv BOD) adsorption on negative and positive SAM layers on
82 gold electrodes was explored. Both the pH of adsorption and the pH for electrocatalysis were
83 systematically varied to modulate the charge of the SAM-gold electrode, the global charge of
84 the protein and the CuT1 vicinity charge. Modeling of cyclic voltammetry curves as well as
85 analysis of DET and MET processes gave access to the distribution of enzyme orientations
86 and enzyme dynamics as a function of pH conditions. Cyclic voltammetry was combined to
87 SPR, PMIRRAS and ellipsometry to correlate the loading and conformation of the
88 biomolecules on the surface to their activity, giving access to a specific activity of the
89 immobilized enzyme. Finally, electrocatalysis at different applied potentials as a function of
90 pH was investigated to prove the effect of electric field on the stability of the bioelectrode.
91 The key parameters obtained for enzyme functional immobilization on planar electrodes will
92 allow determining the next mandatory steps for the development of efficient biotechnological
93 devices.

94

95 **EXPERIMENTAL SECTION**

96 **Chemicals and materials.** Ethanol analytical grade 96% (v/v), 2,2'-azino-bis(3-ethylbenzothiazoline-
97 6-sulfonic acid) (ABTS), 6-mercaptohexanoic acid (6-MHA), 4-aminothiophenol (4-ATP), 11-
98 mercaptoundecanoic acid (11-MUA), sodium hydroxide 97 % (NaOH) and sulfuric acid 95-98 %
99 (H₂SO₄) were purchased from Sigma-Aldrich. Phosphate-Citrate (for pH 3.6 and 4.6) and phosphate
100 (for pH above 5) buffer solutions were prepared by mixing Na₂HPO₄, NaH₂PO₄ and citric acid in an
101 appropriate ratio to obtain pH in the range 3.6–7.5 and a final buffer concentration of 0.1 M. All
102 solutions were prepared with Milli-Q water (18.2 MΩ cm). Bilirubin oxidase from Myrothecium

103 verrucaria (Mv BOD) was a gift from Amano Enzyme Inc. (Nagoya, Japan). Fresh solutions of Mv
104 BOD were prepared in 100 mM phosphate, or phosphate-citrate buffers at the desired pH.

105
106 **Electrode Preparation.** A polycrystalline gold electrode (with a geometric surface of 0.008 cm²) from
107 Bio-Logic Science Instruments was used. Prior to use, the Au electrode was mechanically polished
108 with 1.0, 0.3, and 0.05 μm Al₂O₃ slurry, subsequently followed by intermediate washing with Milli-Q
109 water. After polishing, the electrode was electrochemically cleaned by cycling the applied potential
110 between 0 and 1.35 V in 0.5 M H₂SO₄ at a scan rate of 100 mV.s⁻¹ until a stable voltammogram was
111 obtained (~40 cycles). The electroactive surface area was calculated by integrating the gold oxide
112 reduction peak, taking into account a charge of 390 μC.cm⁻² for the reduction of gold oxide
113 monolayer. The roughness factor, R_f, defined as the ratio of electroactive surface area to projected
114 geometrical surface area ($R_f = A_{\text{electroactive}} / A_{\text{geometric}}$), was determined for each electrode. Values
115 between 2.7-3.2 are determined, allowing to calculate the real electroactive surface. All the currents in
116 this work are reported versus this electroactive surface. Then, the Au electrode was sonicated with 1:1
117 (water-ethanol) solution for 10 min and rinsed twice extensively with water and later with ethanol.
118 Finally, SAMs were formed by incubating the pretreated electrode in 5 mM ethanolic thiol solutions
119 for 15±5 hours. The SAM modified electrodes are named according to the thiol molecule, i.e. 6-MHA-
120 SAM, 4-ATP-SAM, etc. The surface was then cleaned with ethanol to remove all organic
121 contaminants, and finally washed with water and dried under nitrogen flux. Prior to the enzyme
122 immobilization, one CV cycle was done as a blank for thiol-SAM electrode. A reproducible
123 voltammogram at 5 mV.s⁻¹ with capacitive current in the range 0.04-0.06 μA.cm⁻² was observed which
124 reflects that the Au electrode surface is well decorated by thiol molecules.

125 pH dependent electrochemical response from adsorbed enzyme on thiol-SAM modified gold electrode
126 was realized by following two independent approaches. The first approach was based on the enzyme
127 adsorption at different pHs on thiol-SAM electrodes. Unless otherwise indicated the thiol-SAM
128 electrode was incubated in 20 μM Mv BOD solution at the desired pH for 15 min at 4°C. This
129 bioelectrode is named as thiol-SAM/Mv BOD. Then the thiol-SAM/Mv BOD electrode was removed
130 from enzyme solution, gently washed with the same buffer to remove the loosely adsorbed enzymes,

131 and transferred to the electrochemical cell containing enzyme free phosphate buffer (100 mM)
132 saturated with O₂ at a fixed pH 6 as a supporting electrolyte solution for electrocatalysis experiments.

133 In another approach, a thiol-SAM/Mv BOD electrode was prepared by incubating a thiol-SAM
134 electrode in 20 μM Mv BOD solution of fixed pH (100 mM buffer concentration) for 15 min at 4°C.
135 After washing, the thiol-SAM/Mv BOD electrode was transferred to the electrochemical cell
136 containing 100 mM buffer of variable pH as supporting electrolyte solution for electrocatalysis
137 experiments.

138
139 **Electrochemistry measurements.** All electrochemical measurements (Cyclic voltammetry (CV),
140 chronoamperometry and electrochemical impedance spectroscopy) were performed in a standard 3-
141 electrode cell (comprising a polycrystalline gold as a working electrode, a Hg/Hg₂SO₄ reference
142 electrode and a Pt-wire auxiliary electrode) using a potentiostat from Autolab PGSTAT30 controlled
143 by Nova software (Eco Chemie). All potentials are quoted vs Ag/AgCl reference electrode by adding
144 430 mV to the measured potential. The cell was thermostated at 25°C and oxygen was continuously
145 bubbled into the cell throughout the experiments, unless otherwise specified. No significant
146 differences in magnitude and shape of catalytic curves were observed when varying the scan rate
147 (Figure S1), suggesting that the voltammograms are close to the steady-state. At least three to five
148 experiments were conducted in each condition, and only the bioelectrodes whose output current
149 deviation was less than 10% of the average were considered. After DET signal was recorded, 50 μM
150 ABTS was introduced in the solution to detect any MET process. The MET contribution was
151 evaluated by the ratio between DET and (DET+MET) current.

152
153 **Modeling of the cyclic voltammetry curves.** The fitting of electroenzymatic curves was obtained by
154 following the formalism developed by Armstrong and co-workers²⁷:

$$j = \frac{j_{\text{lim}}}{\beta d_0} \frac{e_1 - e_2}{1 + e_1} \ln \frac{pe_1^{\alpha_c} + (1 + e_1)}{pe_1^{\alpha_c} + (1 + e_1)\exp(-\beta d_0)} \quad (1)$$

156 Where $e_1 = \exp((n_1F/RT)(E - E^0_{\text{CuT1}}))$, $e_2 = \exp((-n_2F/RT)(E^0_{\text{CuT1}} - E^{\text{eqm}}_{\text{O}_2/\text{H}_2\text{O}}))$, $p = (k_{2a} + k_{2c})/k_{\text{max}}$.
157 E^0_{CuT1} is the redox potential of the CuT1, $E^{\text{eqm}}_{\text{O}_2/\text{H}_2\text{O}}$ is the equilibrium potential of the O₂/H₂O redox

158 couple, n_1 and n_2 are the numbers of electrons transferred in the electrochemical and enzymatic
159 reactions respectively, and βd_0 is the dispersion parameter. The parameter p describes how proficient
160 the enzymatic electrocatalysis relative to interfacial transfer rate is. The background was subtracted
161 from the CVs prior to the fitting, and Origin 8.5 software was used for the fitting of the half CV cycle
162 within the potential window 0.6-0.1 V vs Ag/AgCl. For the different set of experiments E^{eqm} , was
163 adjusted according to the working electrolyte pH whatever the conditions of adsorption.

164

165 **Spectroscopic assays and protein aggregation measurements.** UV-vis absorption spectra were
166 recorded with a Cary-Win UV spectrophotometer equipped with a Peltier thermostable multicell
167 holder. All spectroscopic data were obtained with Mv BOD in phosphate/phosphate-citrate buffer (100
168 mM) at the desired pH. Same batch of enzyme was prepared and kept at either 4°C or 25°C. In a 500
169 μ L clean cuvette, 10 μ L of 200 nM enzyme, 50 μ L of 20 mM ABTS and 430 μ L of desired buffer
170 were mixed. Then UV-vis spectra were recorded for 60 s. The effect of pH on the BOD activity was
171 examined spectrophotometrically by following the oxidation of ABTS at 420 nm ($\epsilon_{420nm} = 36 \text{ mM}^{-1}$
172 cm^{-1}). All experiments were performed in triplicate, and standard errors were calculated. The mean of
173 the highest activity was set as 100% of the relative activity.

174 The aggregation measurements were done using UV-vis spectrophotometry. Mv BOD was diluted in
175 phosphate/phosphate-citrate buffer at the different pHs to 20 μ M concentration. After 15 minutes
176 incubation at room temperature (RT) or in ice, UV-vis spectra were recorded. Apparition of aggregates
177 was followed overtime by measuring UV-vis absorption at 360 nm at RT.

178

179 **Surface Plasmonic Resonance (SPR).** SPR measurements were acquired on an Autolab SPRINGLE
180 instrument (Eco Chemie, The Netherlands) by using gold disks (25 mm diameter) purchased from Eco
181 Chemie. The thiol modification of the gold disks followed the same procedure as for the Au electrode.
182 For the SPR measurements, 100 μ L of 0.1 M phosphate/phosphate-citrate buffer of desired pH, was
183 injected into the cell until stabilization of the signal was achieved. The buffer solution was then
184 replaced by a solution of 20 μ M Mv BOD in buffer of desired pH, and the SPR signal was monitored
185 to follow enzyme adsorption at RT. At the end of the adsorption process, enzymes remaining in

186 solution and loosely adsorbed molecules were removed from the cell by buffer washing. The
187 procedures for sample injection and removal were carried out using an autosampler (Eco Chemie)
188 equipped with a peristaltic pump.

189 Data were analyzed by a SPR software from Eco Chemie. The mass of the adsorbed species was
190 calculated from the SPR signal on the basis of the relation that a change of 122 mdeg (millidegrees)
191 corresponds to 1.0 ng.mm⁻² at 25°C. For Mv BOD, this means that 100 mdeg of SPR angle
192 corresponds to a coverage of 1.7 pmol.cm⁻². At least four experiments were conducted, and only the
193 electrodes whose surface coverage deviation did not exceed 10% of the average were used. The
194 standard deviation was calculated from the measurements using different electrodes. The mass of the
195 adsorbed species was calculated from the SPR signal on the basis of the relation that a change of 122
196 mdeg (millidegrees) corresponds to 1.0 ng.mm⁻² at 25°C.

197

198 **Ellipsometry.** Variable Angle Spectroscopic Ellipsometry (VASE) has been performed in order to
199 determine the thicknesses of the 6-MHA and 4-ATP based SAMs and the Mv BOD layers as a
200 function of pH. We used a Semilab rotating compensator ellipsometer (RCE) with a microspot which
201 focuses the beam on the sample. The beam diameter is around 100 μm. Data were measured for
202 wavelengths ranging between 350 nm to 600 nm at three different incident angles (65°, 70° and 75°).
203 The Ellipsometry Analysis (SEA) software from the Semilab company was used to fit the VASE
204 measurements and to extract the dielectric functions $\epsilon(\lambda)$ of the materials. This software allows
205 minimizing the mean squared error (MSE) between the measured and the calculated ellipsometric
206 spectra of $\tan(\Psi)$ and $\cos(\Delta)$ thanks to a Levenberg-Marquardt algorithm. Good agreement between
207 the measurements and the calculations were obtained for all incident angles which indicates that the
208 dispersion models are robust and appropriately fits the data. The obtained RMSE from the fits over the
209 whole spectral range and for all incident angles ranges between 0.01 and 0.018 for all samples.

210 The dielectric function of gold has been fitted using Drude-Lorentz oscillators combined with a
211 Sellmeier model. Drude-Lorentz oscillators are suitable for the dielectric constant determination of
212 metals²⁸. A Sellmeier model has been added in order to take into account the presence of H₂O
213 molecules in the gold porosities when the substrates are introduced in the solutions. The dielectric

214 function of each gold substrate has been determined since it can weakly change from a sample to
215 another one. The same dielectric function model has been used for the 6-MHA based SAMs and the
216 Mv BOD layers. A Sellmeier model has been used to describe such non absorbing dielectric materials.
217 The obtained refractive index is quasi-constant around 1.48 as a function of the wavelength which is
218 very close to a previously reported value ($n=1.45$)²⁹.

219 For the VASE measurements, the samples were first plunged overnight in the thiol solutions in order
220 to self assemble the 6-MHA monolayers on gold, then in the enzyme solution to adsorb the Mv BOD
221 on the 6-MHA-SAM at 4°C for 15 min. Then, the samples were washed with buffer, then with water.
222 Finally, the samples were carefully dried under mild nitrogen flux before performing the VASE
223 measurements in air. The thickness was measured at three different positions on the sample. The
224 thicknesses of the 6-MHA-SAM and 4-ATP-SAM were measured as 0.7 ± 0.05 nm and 0.72 ± 0.06 nm,
225 respectively.

226

227 **PMIRRAS measurements.** Gold mirrors from Optics Balzers were used for PMIRRAS
228 measurements. SAMs were formed by incubating the gold mirrors in 5 mM ethanolic thiol solutions
229 for one night. The surface was then cleaned with ethanol to remove all organic contaminants, and
230 finally washed with water and dried under nitrogen flux. The thiol-SAM functionalized gold surface
231 was incubated in 20 μ M Mv BOD solution at 4°C and at the desired pH for 15 min. To evaluate the
232 effect of pH on the conformation of the immobilized enzyme, the thiol-SAM/Mv BOD gold surface
233 was immersed in various pH buffers during 15 min.

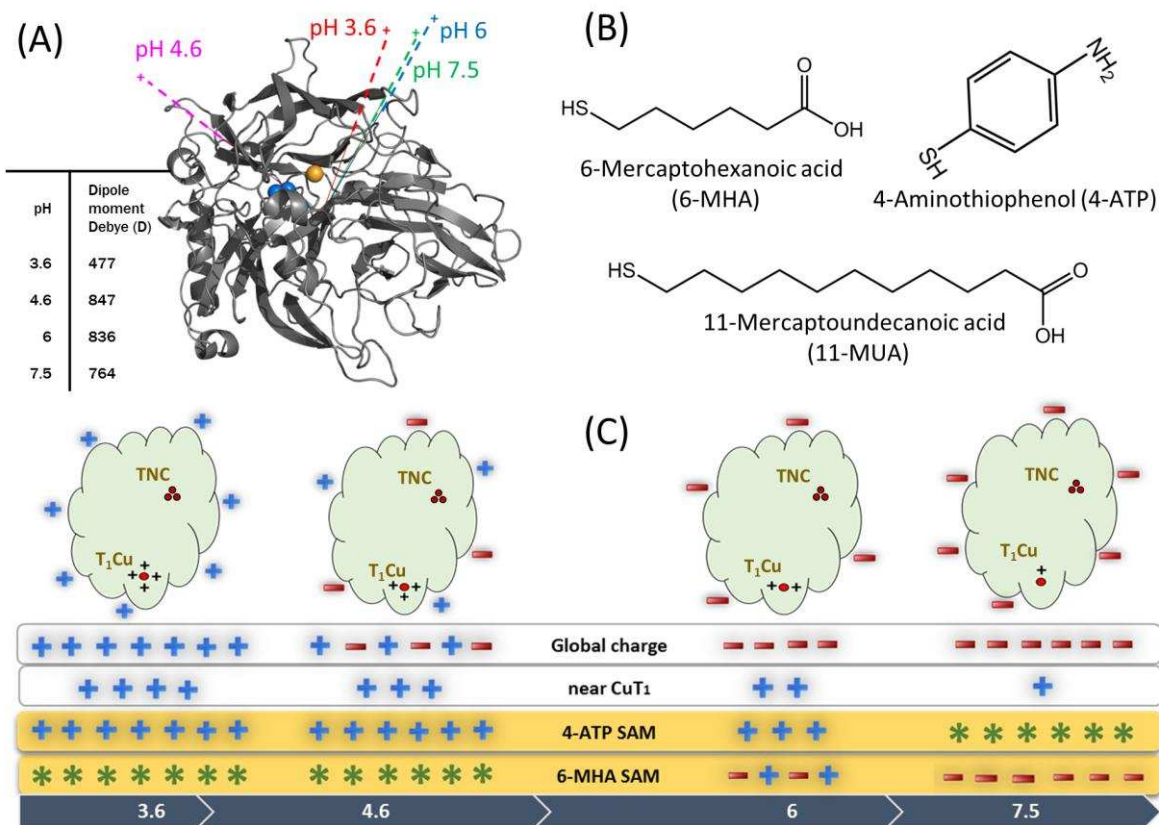
234 For PMIRRAS analyses, the surface was cleaned with milli-Q water to remove salts present in the
235 buffer, and finally the surface was dried. The modified dried gold electrode was placed at RT in the
236 external beam of a Nicolet Nexus 870 FT-IR spectrometer (Madison, WI), and the reflected light was
237 focused on a nitrogen-cooled (77 K) HgCdTe (MCT) detector (SAT, Poitiers). The optimal value of
238 the angle of incidence for the detection was 75° relative to the optical axis normal to the interface. A
239 ZnSe polarized grid and a ZnSe photoacoustic modulator to modulate the incident beam between p
240 and s polarizations were placed before the sample. The detector output was sent to a two-channel

241 electronic device that generated the sum and the difference interferograms. The PMIRRAS spectra
242 were recorded at 8 cm^{-1} resolution, with coaddition of 600 scans. Using a modulation of polarization
243 enabled us to perform rapid analyses of the sample after treatment in various solutions without purging
244 the atmosphere or requiring a reference spectrum. Protein adsorption can be attested by the presence of
245 the amide I (mainly C=O stretching vibrational mode) and the amide II (mainly N-H stretching
246 vibrational mode) at around 1660 and 1540 cm^{-1} , respectively ¹⁶. Subtraction of the thiol-SAM spectra
247 from the thiol-SAM/Mv BOD was realized for PMIRRAS data analysis.

248

249 **RESULTS AND DISCUSSION**

250 **SAMs and Mv BOD charges as a function of pH.** Four different pHs were used throughout
251 this work: 3.6, 4.6, 6 and 7.5. In this pH range, both the protein and the electrode charges
252 vary. Concerning Mv BOD, the theoretical global charge of the protein is slightly positive
253 (+10) at pH 3.6, almost neutral at pH 4.6, and negative at the other pHs ¹⁵. We calculated in
254 this work a dipole moment around 800 Debye for the protein at pH 7.5, 6 and 4.6, while the
255 value of the dipole moment decreases to less than 500 Debye for pH 3.6. The direction of the
256 dipole moment points towards the CuT1 at pH 7.5 and pH 6, while its direction is shifted at
257 pH 4.6 (Figure 1A). From our previous work, the charge in a sphere of 15 \AA around the CuT1
258 is neutral at pH 7.5, slightly positive at pH 6 (+2) and displays a net positive value at pH 4.6
259 and 3.6 ¹⁵. Both charge distributions are important for Mv BOD adsorption. The protein global
260 charge is expected to control the repulsive or attractive interaction between the enzyme and
261 the electrode, i.e. the strength of adsorption, while the local charge around the CuT1 may
262 control the orientation of the protein for DET. Two types of thiol-based SAMs were
263 investigated in this work to tune the electrostatic interactions (Figure 1B): 6-MHA and 11-
264 MUA both carry carboxylic end-functions, and 4-ATP carries an amino group. As a function
265 of pH, these SAM electrodes will present either positive, or negative or neutral charges
266 depending on the pKa of the chemical end-function ³⁰.



267
 268 **Figure 1. Charges of Mv BOD and of the thiol-based SAMs as a function of pH.** (A) Mv BOD
 269 structure and dipole moments at pH 7.5, 6, 4.6 and 3.6. Blue spheres correspond to copper atoms
 270 involved in the trinuclear center, and the gold sphere corresponds to the CuT1. Dipole moments are
 271 calculated with Protein Dipole Moments Server³¹, from structure prepared at different pHs with the
 272 PDB2PQR-Propka Server³² using the Parse force fields. Illustration is performed with Pymol (The
 273 PyMOL Molecular Graphics System, Version 1.8 Schrodinger, LLC); (B) Formula of 6-MHA, 11-
 274 MUA, and 4-ATP; (C) Scheme illustrating the global charge of the Mv BOD enzyme, the charge
 275 around the CuT1 and the charges of 6-MHA-SAM and 4-ATP-SAM electrodes, as a function of pH.
 276 Green stars represent a neutral surface.

277
 278 The pKa of thiols involved in SAMs is a function of the number of carbons forming the linear
 279 chain³³. The pKa of 4-ATP was previously determined to be 6.9³⁴. In the case of the
 280 carboxylic terminated alkanethiols, it is known that the pKa of the surface thiols is higher than
 281 in solution as a result of the interactions between the thiol molecules in the SAM. The pKa of

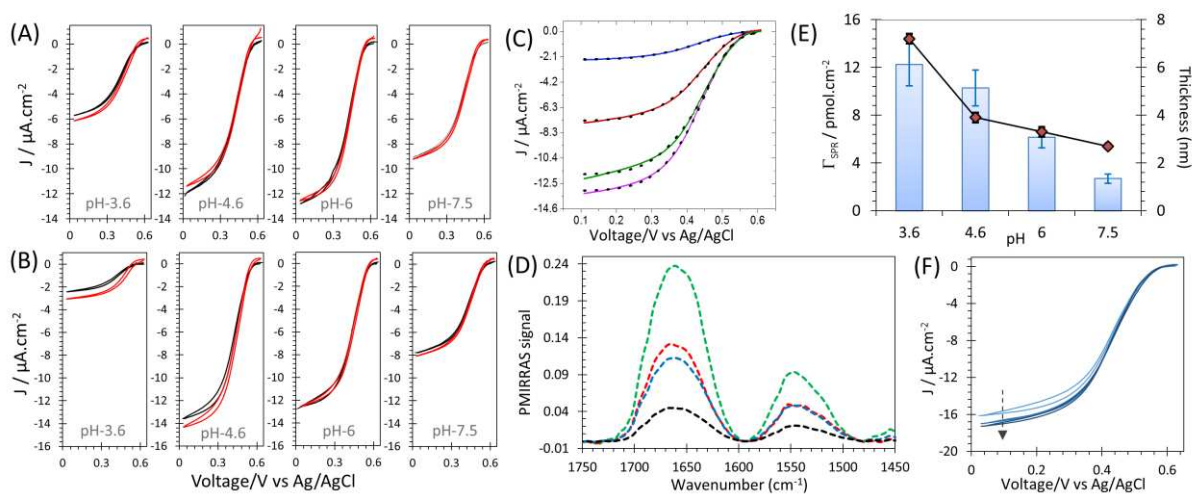
282 11-MUA-SAM was reported to be around 6²⁶. In this work, we determined by impedance
283 spectroscopy a pKa value close to 6 for 6-MHA-SAM (Figure S2). According to the statement
284 made above, the comprehensive Figure 1C allows to envision pH zones for repulsive or
285 attractive interactions between the enzyme and the SAM layer expected to control enzyme
286 loading. It also permits to predict pH zones for which orientation of the protein for DET is
287 expected to be favored as a function of the SAM chemistry.

288

289 **Influence of the pH of adsorption of Mv BOD on 6-MHA-SAM.** Mv BOD adsorption was
290 carried out at 4°C on 6-MHA-SAM at the 4 different pHs, while recording the electroactivity
291 at pH 6 and 25°C. Following this protocol, the intrinsic activity of enzymes adsorbed on SAM
292 is fixed during the electrochemical experiments. The CV responses should have a direct
293 dependence on enzyme loading and on the enzyme-SAM/enzyme-enzyme interactions that
294 come into play at the electrochemical interface, both during the adsorption step and upon
295 transfer to pH 6. Not only DET but also MET were quantified for each pH of adsorption. In
296 addition, SPR and ellipsometry measurements as well as PMIRRAS spectra were recorded
297 after enzyme adsorption at the four different pHs, to correlate the activity with the amount and
298 conformation of the enzymes (Figure 2).

299 Independently of the pH of adsorption, DET occurs when the bioelectrode is transferred from
300 a given pH to pH 6 (Figure 2A and Figure 2B). A sigmoidal wave develops in the presence of
301 O₂, with an onset potential around 0.55 V suggesting a catalysis driven by the CuT1¹⁵⁻¹⁶. The
302 value of DET current density depends however on the pH of adsorption in the range: I_{DET} pH
303 3.6 < I_{DET} pH 7.5 < I_{DET} pH 4.6 ≈ I_{DET} pH 6. The DET current did not show any drastic
304 variation between 1 and 15 min of adsorption, except for pH 3.6 where it is twice less after 15
305 min of adsorption compared to 1 min of adsorption. The CV shapes and modeling indicate

306 that enzyme orientation distribution on 6-MHA-SAM is more or less identical irrespective of
 307 the adsorption pH, with βd_0 values close to 5 (Figure 2C and Table 1).



308
 309 **Figure 2. Correlation between electroactivity, orientation, conformation and loading of Mv BOD**
 310 **adsorbed at different pHs on carboxylic-based-SAMs.** CVs of O₂ reduction at pH 6 and 25°C by
 311 Mv BOD adsorbed on 6-MHA-SAM at different pHs at 4°C after (A) 1 min and (B) 15 min of
 312 adsorption. Black lines and red lines are obtained before and after 50 μ M ABTS addition in solution,
 313 respectively. 0.1 M phosphate buffer, $v = 5 \text{ mV}\cdot\text{s}^{-1}$. (C) Modeling of the electrochemical signal.
 314 Electrocatalytic CV curves at pH 6 obtained at different adsorption conditions (solid line) and curves
 315 fitted according to equation 1 (See experimental section) (dotted line): pH 3.6 (blue), pH 4.6 (purple),
 316 pH 6 (green), pH 7.5 (red). (D) PMIRRAS spectra of Mv BOD adsorbed on 6-MHA-SAM. The gold
 317 modified surface was placed in 20 μ M Mv BOD solution at pH 7.5 (black line), pH 6 (blue line), pH
 318 4.6 (red line) and pH 3.6 (green line) during 15 min and was then immersed in phosphate buffer at pH
 319 6 during 30 min at 4°C. The gold modified electrodes were rinsed and dried in order to record
 320 PMIRRAS spectra. (E) Enzyme coverage and enzyme layer thickness as a function of pH after
 321 adsorption of 20 μ M Mv BOD at RT during 15 min on 6-MHA-SAM. Enzyme coverage (blue bars)
 322 was obtained by SPR and enzyme layer thickness (\blacklozenge) was measured by ellipsometry. (F) Increase in
 323 the consecutive CV catalytic currents at pH 6 after adsorption of 20 μ M Mv BOD on 6-MHA-SAM in
 324 pH 4.6 buffer for 15 min at 4°C.

325

326 The amide I/amide II ratio on the PMIRRAS spectra is also the same whatever the pH (i.e. 3.2
327 ± 0.1 , 3.1 ± 0.1 , 3.0 ± 0.2 , 2.9 ± 0.6 at pH 3.6, 4.6, 6 and 7.5 respectively) (Figure 2D).
328 However, we already reported that the distribution and orientation of structural components in
329 Mv BOD could yield to similar amide I/amide II ratio despite different orientations in the
330 immobilized state¹⁶. ABTS as a redox mediator was thus added into the electrolyte to further
331 evaluate the orientation of the enzyme at a given pH. In the case of pH 3.6, a clear MET
332 signal can be observed corresponding to 20% of the total catalytic signal. But at the other pHs
333 of adsorption, MET current is either zero or less than 5 % (Figure 2A and Figure 2B, red
334 lines), in accordance with a narrow enzyme distribution.

335 Catalytic current relative magnitude can be ascribed either to a different amount of loaded
336 enzymes with similar ET rates, or to different ET rates of similar amount of proteins
337 adsorbed. Change in enzyme orientation or modification of enzyme conformation can affect
338 the ET. The appearance of the amide bands at the same wavelength in the PMIRRAS spectra
339 irrespective of the adsorption pH, demonstrates that there is no change in the secondary
340 structure of the enzyme (Figure 2D). Similar values of βd_0 further suggest that the loading of
341 enzymes should be more critical than the orientation of the enzyme. Accordingly, PMIRRAS
342 spectra and SPR signals indicate an increase in the enzyme amount adsorbed on the 6-MHA-
343 SAM with decreasing pHs, which correlates with an increase of the enzyme layer thickness
344 measured by ellipsometry (Figure 2D, Figure 2E and Figure S3). After 15 min of adsorption,
345 values of 2.7 ± 0.39 , 6.2 ± 0.89 , 10.3 ± 1.5 , and 12.2 ± 1.78 pmol.cm⁻² were obtained from the SPR
346 angle deviations at pH 7.5, 6, 4.6 and 3.6 respectively. Considering that a theoretical
347 monolayer of Mv BOD should be between 4.6 and 10.4 pmol.cm⁻² depending on the
348 conformation the enzyme takes upon immobilization (Mv BOD dimensions are $4 \times 5 \times 6$ nm³)³⁵,
349 a monolayer is not obtained at pH 7.5. More than one monolayer is formed at pH 3.6, which is
350 traduced in an enzyme layer thickness larger than the protein dimension.

351 **Table 1. Values of the parameter βd_0 for distribution of enzyme orientation.** Values of βd_0 are
 352 obtained from the modeling of CV curves in Figure 2 (adsorption of Mv BOD on 6-MHA-SAM at
 353 different pHs and electroactivity at pH 6) and Figure 4 (adsorption of Mv BOD on 6-MHA-SAM at pH
 354 6 and electroactivity at different pHs). For comparison, βd_0 values obtained by modeling of CVs of O₂
 355 reduction by 20 μ M Mv BOD adsorbed on bare gold at pH 6 are also given.

pH	Orientation parameter βd_0		
	SAM (6-MHA)		Bare Gold
	Adsorption at different pH	Adsorption at pH 6	Adsorption at pH 6
3.6	5.1 \pm 0.15	12.8 \pm 0.05	9.6 \pm 0.30
4.6	3.9 \pm 0.15	10.6 \pm 0.12	9.8 \pm 0.08
6	4.9 \pm 0.19	4.9 \pm 0.18	10.9 \pm 0.66
7.5	5.1 \pm 0.16	6.8 \pm 0.17	*

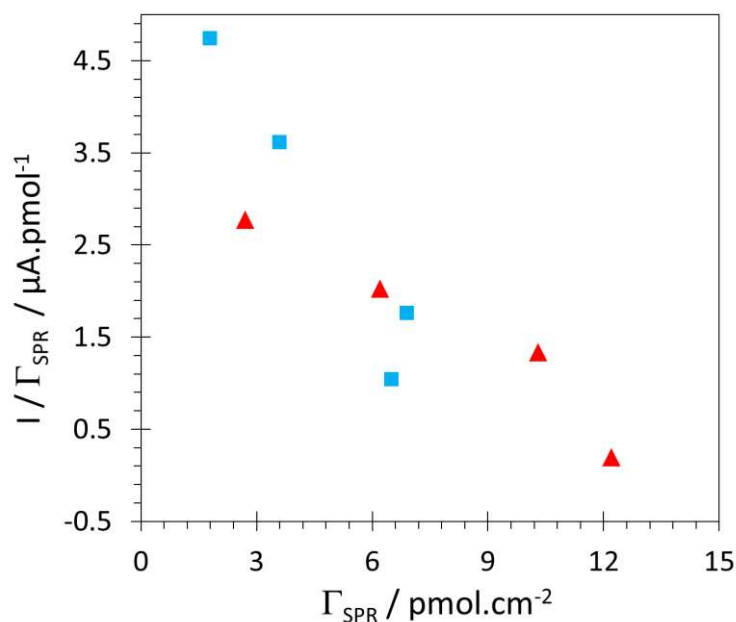
* No DET due to low activity of enzyme

356
 357
 358 The magnitude of the catalytic current and the loading of enzymes observed as a function of
 359 the pH of adsorption can be explained based on the respective charges of the protein, the
 360 environment of the CuT1 and the SAM. At pH 7.5, repulsive electrostatic interactions
 361 between the negatively charged protein and the negative SAM should prevent BOD
 362 adsorption. In accordance, less than one monolayer of enzyme is obtained. Nevertheless, the
 363 neutral environment around the CuT1, associated to a high dipole moment (764 Debye)
 364 pointing toward the CuT1¹⁵, enables BOD adsorption via the CuT1. Hence, DET but no MET
 365 is observed. The enzyme thickness obtained by ellipsometry (2.7 \pm 0.1 nm) (Figure 2E)
 366 suggests however some flattening of the enzyme. Compared to pH 7.5, the most prominent
 367 change at pH 6 is the lowest negative charge of the SAM. As a consequence, the amount of
 368 molecules adsorbed is more than twice higher than at pH 7.5, the enzyme layer thickness is
 369 increased (3.3 \pm 0.2 nm), leading also to a higher direct catalytic current than when adsorption
 370 is made at pH 7.5. At pH 4.6, the amount of adsorbed proteins is enhanced compared to pH 6

371 because the repulsive interactions are now weak between the protonated SAM and neutral Mv
372 BOD. A coverage close to the maximum theoretical coverage is obtained. Ellipsometry gives
373 an enzyme thickness of 3.9 ± 0.2 nm, very close to the geometrical enzyme dimension. The
374 direction of the dipole moment at pH 4.6 which does not point anymore to the T1 should lead
375 to a higher distribution of orientation. However, MET contribution is low, and βd_0 value
376 suggests a narrow distribution of orientation, very similar to pH 6 (Figure 2 and Table 1).
377 Two main hypotheses can be proposed. Either the electrostatic interactions between the Cu T1
378 and the SAM, although weak, are sufficient to induce a major DET orientation of the enzyme
379 on the surface, or mobility of the protein allows it to adopt a favorable orientation for DET
380 upon transfer to pH 6. The later hypothesis is supported by the increase in the DET current
381 during the first three cycles, before reaching the maximum current as a consequence of
382 progressive reorientation (Figure 2F).

383 The second main conclusion from our experimental results is that a higher enzyme loading
384 does not translate directly in a higher catalytic activity. The specific activity defined as the
385 ratio of the DET current by the enzyme coverage has been calculated at all the pHs of
386 investigation. It is reported in Figure 3 as a function of the enzyme coverage. This analysis
387 underlines that the highest specific activity is obtained for the lowest coverage. As developed
388 by Blanford and coworkers³⁶, less steric hindrance because of lower coverage may be the
389 reason for a higher specific activity.

390



391
 392 **Figure 3. Relation between enzyme coverage and electroactivity.** Dependence of the specific
 393 enzyme electroactivity on the enzyme coverage after 1 min (■) or 15 min (▲) of Mv BOD adsorption.
 394 Enzyme coverage is obtained from the SPR angle at the different pHs at RT, catalytic currents are
 395 measured at 0 V vs Ag/AgCl at pH 6 and RT. The enzyme adsorption for electrochemistry was made
 396 at 4°C.

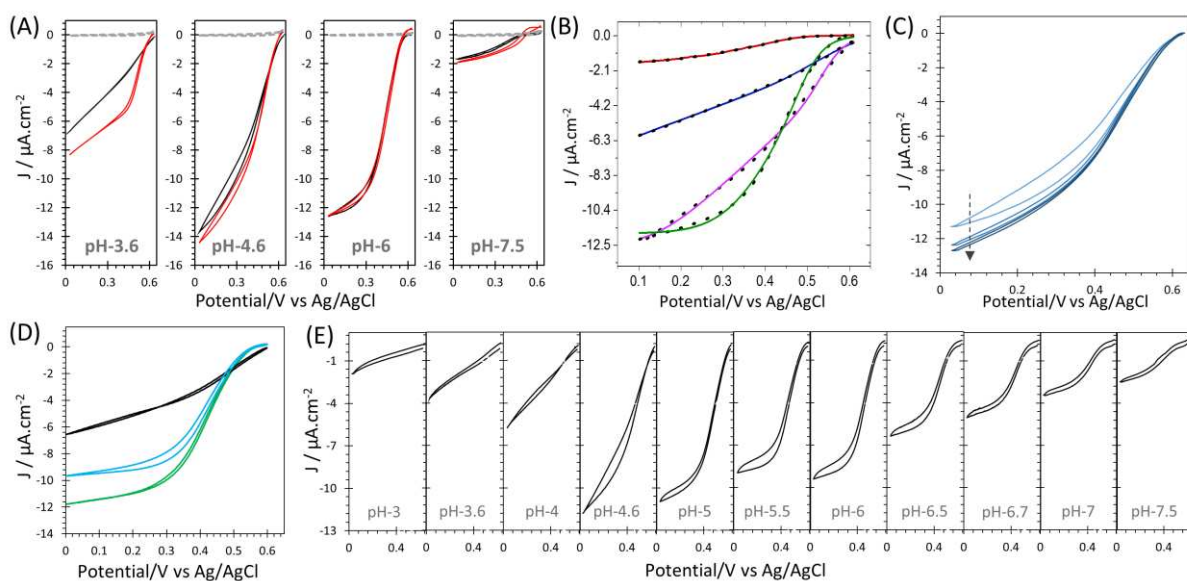
397
 398 The case of pH 3.6 is noteworthy to be discussed apart from the other investigated pHs. At
 399 this pH, the weak interaction between the positively charged enzyme and the protonated
 400 SAM, in addition to a much lower dipole moment (477 Debye) is expected to yield a high
 401 degree of mobility of the enzyme, which can adopt many orientations. Although this is the
 402 only case where MET contributes to the whole catalytic signal (Figure 2), DET remains the
 403 major process, and βd_0 value reflects a narrow distribution of orientations (Table 1). Protein
 404 dynamics upon transfer of the bioelectrode from pH 3.6 to pH 6 may explain a favored DET
 405 process. Both the amount of protein and the layer thickness measured by ellipsometry are
 406 indicative of the formation of more than one monolayer (Figure 2E). The occurrence of a
 407 MET process at pH 3.6 can thus be attributed to enzyme multilayers rather than to a

408 distribution of orientation. Despite the highest amount of proteins, the lowest catalytic current
409 is obtained. The stability of the enzyme is also the lowest at this pH, as highlighted by the
410 homogeneous activity reported in Figure S4, where only 20% of the activity is recovered after
411 1 hour of storage. Acidic pH conditions, mostly below pH 3, are known to cause protein
412 unfolding as a result of intramolecular charge repulsion³⁷. In this work, aggregate formation
413 was effectively observed at pH 3.6 and RT (Figure S5). However, similar enzyme layer
414 thickness values (around 7.2 nm) were obtained by ellipsometry after adsorption at pH 3.6
415 either at 4°C or at RT, and PMIRRAS spectra indicated that there is no change in the
416 secondary structure of the protein adsorbed at pH 3.6. Thus, aggregation process might not be
417 the major contribution to the low direct catalytic current when adsorption is made at pH 3.6,
418 which would be more related to steric hindrance between proteins in the layer. Interestingly,
419 when adsorption was made at RT at pH 3.6, conditions favoring protein aggregation, the
420 direct electrochemical signal magnitude recorded at pH 6 was four times higher than when the
421 adsorption was made at 4°C (Figure S5). Although it is reported that cross-linked enzyme
422 aggregates (CLEA) of laccases may remain active and stable³⁸, control experiments in this
423 work showed that unfolded or denaturated proteins do not induce any electrocatalytic signals
424 (Figure S6 and Figure S7). The following hypotheses could thus explain this particular
425 behavior: (i) protein aggregation occurring at RT might remove some BOD population not
426 well folded, and consequently increases the specific catalytic electroactivity, (ii) the presence
427 of aggregated proteins adsorbed on the electrode could optimize the enzyme wiring, playing
428 the role of cross-linkers

429 .

430 **Varying the pH of electroactivity.** The adsorption of Mv BOD on 6-MHA-SAM was
431 alternatively carried out at pH 6 for 15 min at 4°C, then the Mv BOD/6-MHA-SAM was
432 transferred to buffers at the different pHs 3.6, 4.6, 6 or 7.5, respectively. The typical CVs for

433 electroenzymatic O₂ reduction are shown in Figure 4A where both DET and MET signals are
434 overlaid.



435
436 **Figure 4. pH-induced dynamics of Mv BOD on 6-MHA-SAM.** (A) CVs of O₂ reduction by 20 μM
437 Mv BOD adsorbed on 6-MHA-SAM at 4°C and pH 6 for 15 min and transferred to different pHs for
438 catalysis measurement (black curves). Red curves are obtained after 50 μM ABTS addition, and grey
439 dotted curves correspond to the SAM alone; (B) Modeling of the electrochemical signal.
440 Electrocatalytic CV curves at different pHs after adsorption at pH 6 (solid line) and curved fitted
441 according to equation 1 (dotted line) (see experimental section). Mv BOD was adsorbed on 6-MHA-
442 SAM at pH 6 and electrochemistry was recorded at different pHs: pH 3.6 (blue), pH 4.6 (purple), pH 6
443 (green), pH 7.5 (red). (C) Increase in the consecutive CV catalytic currents at pH 4.6 after 20 μM Mv
444 BOD was adsorbed on 6-MHA-SAM in pH 6 buffer for 15 min at 4°C. (D) CVs for O₂ reduction by
445 Mv BOD adsorbed on 6-MHA-SAM at 4°C after multiple steps of transfers: adsorption at pH 6 for 15
446 min, measurement at pH 6 (green), washing step then transfer and measurement at pH 3.6 (black),
447 washing step then transfer back to pH 6 (blue); (E) CVs of direct O₂ reduction on a full pH range by
448 20 μM Mv BOD adsorbed at pH 6 during 15 min at 4°C. Phosphate citrate buffer (pH 3 to 5.5) or
449 phosphate buffer (pH 6 to 7.5). $v = 5 \text{ mV}\cdot\text{s}^{-1}$.

450

451 Switching the pH of the electrolyte changes simultaneously two parameters, i.e. the intrinsic
452 activity of the enzyme as well as the interaction between Mv BOD pre-adsorbed at pH 6 and
453 the SAM. A first observation is that the catalytic current mainly reflects the activity of the
454 enzyme in solution measured by UV-Vis spectroscopy (Figure S4). Hence, much lower
455 activity is obtained at pH 7.5 compared to the other pHs. As expected, the onset for O₂
456 reduction decreases as pH increases displaying a slope close to 60 mV. The second
457 observation is that the shape of the CV curve is markedly different at pH 3.6 and 4.6
458 compared to pH 6 and 7.5, suggesting a larger distribution of ET rates, linked to a distribution
459 of enzyme orientation. The modeling of the CV curves gave access to the orientation
460 parameter βd_0 , which takes values of 12.8, 10.6 and 4.9 for pH 3.6, 4.6 and 6 respectively,
461 showing a large distribution of orientation at pH 3.6 and pH 4.6, and a narrow one at pH 6
462 (Figure 4B and Table 1). In accordance, MET currents were only observed at pH 3.6 and 4.6,
463 although it cannot be excluded that the magnitude of the MET signal reflects the better
464 affinity of BOD towards ABTS at low pH³⁹, as attested by the decrease of the Michaelis-
465 Menten constant (Figure S8). These results can be explained based on the weak interactions
466 between the SAM and the protein at acidic pHs as discussed above. But this implies also some
467 mobility of the enzyme when transferring the bioelectrode from pH 6 to lower pHs.
468 Accordingly, the catalytic current increased during the first three cycles before reaching the
469 maximum current (Figure 4C). Protein dynamics is further confirmed by experiments
470 involving multiple transfer steps from one pH to another pH. As seen in Figure 4D, the
471 changes in the CV shapes and current magnitude clearly reflect the reversible changes in the
472 distribution of orientation between pH 6 and pH 3.6. Little less current output at the end of the
473 process could be related to loss of some enzymes in the successive transferring steps. The full
474 range of pH was finally investigated after Mv BOD adsorption at pH 6, showing that the
475 electrochemical response can be easily tuned and reflects enzyme activity and dynamics

476 yielding favorable/unfavorable interaction between the enzyme and the SAM layer for DET
477 (Figure 4E).

478

479 **Influence of the SAM chemistry.** To confirm the electrostatic model established from the
480 electrocatalysis on 6-MHA-SAM, we performed adsorption of Mv BOD on other surfaces: (i)
481 11-MUA-SAM, a carboxylic-thiol with 11 carbons in the alkane chain (pKa of 11-MUA on
482 SAM has been reported to be 6), and (ii) 4-ATP, an amino-thiol. After Mv BOD adsorption at
483 pH 6 on 11-MUA-SAM, a DET process is observed when the activity is measured at pH 6,
484 with a lower ET rate than on 6-MHA-SAM, as a consequence of the decrease of the electron
485 tunneling rate with the length of the alkane-chain⁴⁰ (Figure S9). As the chemical functions
486 are identical on 11-MUA and 6-MHA, the charges as a function of pH are also similar. Then,
487 the occurrence of DET over MET process on 11-MUA is based on the same assumption as for
488 6-MHA.

489 The pKa of 4-ATP was reported to be 6.9. Hence, the SAM is positively charged at pH 3.6,
490 4.6 and 6, and neutral at pH 7.5. Except at pH 3.6, electrostatic interactions with the globally
491 negatively charged Mv BOD must favor enzyme approach. As revealed by the SPR data and
492 confirmed by PMIRRAS and ellipsometry measurements (Table 2, Figure 5A and Figure 5B),
493 Mv BOD is adsorbed at pH 6 or at pH 4.6 on 4-ATP-SAM, with similar amounts, reaching a
494 full coverage after 15 min of adsorption. As expected, the amount of loaded enzyme is the
495 lowest at pH 7.5 as a result of lower electrostatic interactions, but higher than on 6-MHA-
496 SAM where repulsive interactions took place. A high amount of proteins is loaded at pH 3.6
497 despite repulsive interactions which may be ascribed to some aggregation process. The band
498 corresponding to the amide I on the PMIRRAS spectra is slightly shifted toward higher wave
499 numbers in comparison with the adsorption on 6-MHA-SAM (Figure 5B). This change can be

500 ascribed to a small opening of the β -sheets that become turn, and suggests, as in the case of
 501 pH 7.5 on 6-MHA-SAM, that stronger electrostatic interactions may destabilize the enzyme.

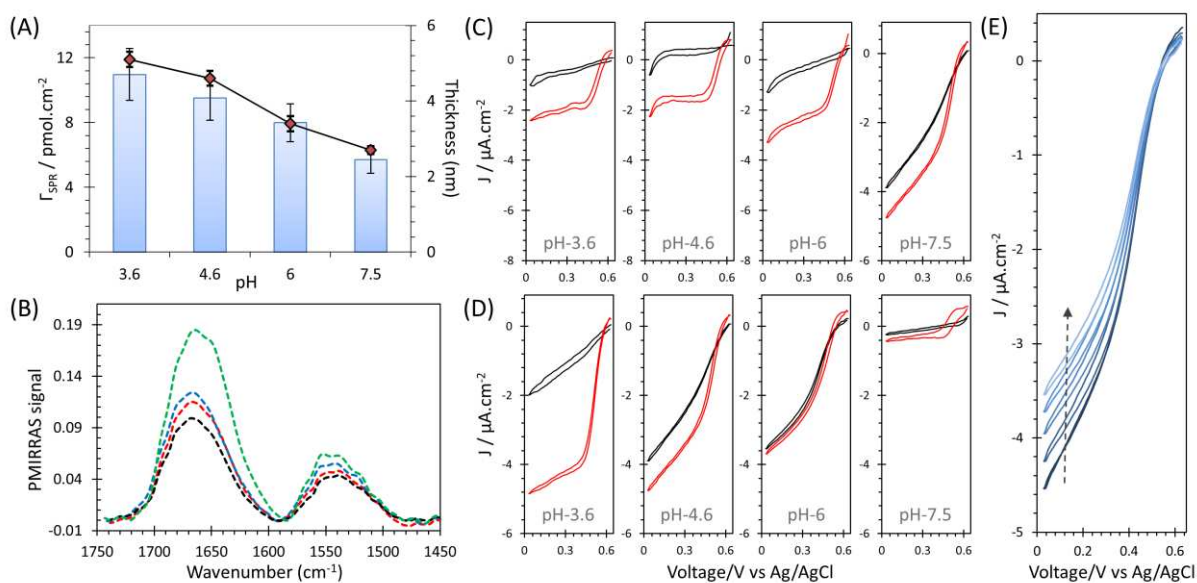
502

503 **Table 2.** SPR data for different pH of Mv BOD adsorption during 15 min on 4-ATP, and values of the
 504 ratio DET/DET+MET at different pHs. The ratios are measured at $E = +120$ mV vs Ag/AgCl.

pH of ads.	4-ATP			
	$\Gamma_{\text{SPR}} / \text{pmol.cm}^{-2}$	$I_{\text{DET}}/I_{\text{DET+MET}}$		
		pH 3.6	pH 4.6	pH 6
3.6	10.97 ± 1.6	0.10	0.36	0.50
4.6	9.5 ± 1.4	0.04	0.23	0.31
6	8.0 ± 1.2	0.06	0.30	0.58
7.5	5.7 ± 0.8	0.38	0.80	0.97

505

506



507

508 **Figure 5. Correlation between electroactivity, conformation and loading of Mv BOD adsorbed**

509 **on amino-based SAM.** (A) Enzyme coverage obtained by SPR (blue bars) and enzyme layer

510 thickness obtained by ellipsometry (\blacklozenge) on 4-ATP-SAM as a function of pH after 15 min of adsorption

511 of $20 \mu\text{M}$ Mv BOD at RT; (B) PMIRRAS spectra of Mv BOD adsorbed on 4-ATP-SAM. The gold

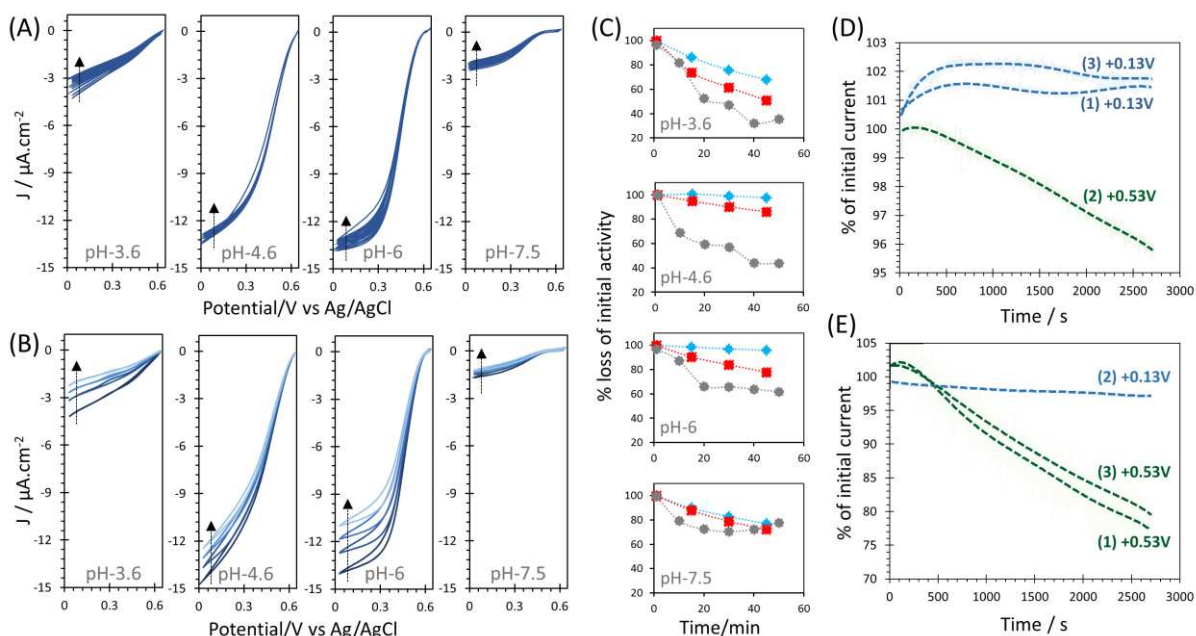
512 modified electrode was placed in solution of $20 \mu\text{M}$ Mv BOD at pH 7.5 (black line), pH 6 (blue line),

513 pH 4.6 (red line), and pH 3.6 (green line) during 15 min at 4 °C, and then immersed in phosphate
514 buffer at pH 6 during 30 min at 4°C; Catalytic O₂ reduction (C) at pH 4.6 after Mv BOD adsorption in
515 the different pH buffers, or (D) in different pHs after 20 μM Mv BOD adsorption at pH 7.5. (E)
516 Decrease in the catalytic current at pH 6 along with CV cycling for bioelectrodes prepared in
517 experiment (D). Black curves and red curves are obtained before and after 50 μM ABTS in solution,
518 respectively. $v = 5 \text{ mV}\cdot\text{s}^{-1}$.

519
520 Figure 5C shows the CVs for O₂ catalytic reduction at pH 4.6 by Mv BOD adsorbed at the
521 different pHs before and after ABTS addition. As a result of the electrostatic model which
522 postulates that the electron transfer process is driven by the positive environment of the CuT1,
523 no DET can be observed when the adsorption is made on the positively charged 4-ATP-SAM
524 at pH 3.6, 4.6 and 6. A MET current develops with a similar magnitude whatever the pH of
525 adsorption, underlining that the total amount of electroactive enzymes is similar (Table 2).
526 Also, in good agreement with the model, a DET signal is obtained at pH 7.5, thanks to
527 dynamics of the protein when transferred to a pH where 4-ATP-SAM is neutral. When the
528 adsorption is made at pH 7.5, DET markedly occurs at pH 6 and pH 4.6 (Figure 5D). This
529 behavior has never been reported before, and underlines the original benefit of the protocol
530 used in this work. The DET catalytic process is not stable with time however, as a result of
531 mobility of the protein upon transfer to pHs where the SAM becomes positively charged
532 (Figure 5E).

533
534 **Catalytic stability and effect of applied potential.** One main issue when dealing with
535 enzyme-based bioelectrodes is the long-term stability. Decrease in electrocatalytic signals
536 may be associated to different phenomena including stability of the enzyme itself, enzyme
537 leakage from the electrochemical interface, changes in orientation and/or in the conformation

538 of the enzyme in the immobilized state. Recent reports coupling electrochemistry to QCM ⁴¹
 539 or SPR ¹⁶ established that the decrease of the catalytic signal for O₂ reduction by Mv BOD
 540 adsorbed on SAM layers, was not linked to enzyme loss from the electrode. Although the
 541 electric field effect on bioelectrode efficiency and stability is not well established, some other
 542 works concluded that decrease in the catalytic activity could be related to changes of the
 543 enzyme layer upon applied potential ⁴¹⁻⁴³.
 544 To evaluate the effect of electrostatic interactions on the stability of the DET signal, we
 545 cycled during 45 min at different pHs the bioelectrode built by Mv BOD adsorbed at pH 6 on
 546 6-MHA-SAM (Figure 6A).



547
 548 **Figure 6. Stability of 6-MHA-SAM/Mv BOD, effect of applied potential.** Stability of the catalytic
 549 O₂ reduction in different pHs by Mv BOD adsorbed on 6-MHA-SAM at pH 6 and 4°C during 15 min.
 550 (A) continuous CV cycling during 45 min; (B) one cycle every 1000 s holding the electrode at OCP
 551 between the cycles; (C) comparative activity loss between (◆) continuous cycling, (■) one cycle
 552 every 1000 s and (●) homogeneous catalysis; (D) and (E) effect of applied potential on the stability of
 553 the catalytic current. Mv BOD adsorbed on 6-MHA-SAM at pH 6, and chronoamperometry recorded
 554 at pH 4.6 (D) or pH 6 (E) at +0.13 V (blue lines), or +0.53 V (green lines), with the sequence denoted
 555 within brackets.

556

557 The percentage of activity loss within 45 min of continuous cycling at RT between 0.6 and 0
558 V vs Ag/AgCl was 30%, 2%, and 4%, respectively at pH 3.6, 4.6, and 6. Compared to the
559 stability obtained in solution at RT (Figure 6C and Figure S4), enzyme immobilization onto
560 the electrode surface greatly enhances the stability, except in the case of pH 7.5, where
561 heterogeneous or homogeneous catalytic stability is similar (20% against 25%). This latter pH
562 is the case where the repulsive interactions between the enzyme and the SAM are the highest,
563 yielding possible losses of proteins by desorption. SPR measurements confirm this hypothesis as
564 25% of the adsorbed proteins are removed away after the rinsing step at pH 7.5 against 5% at pH 3.6
565 and around 10 % at pH 4.6 and 6. But pH 7.5 is also the condition where the electrostatic
566 interactions between the CuT1 and the SAM are the highest. Progressive irreversible change
567 in the structure of the enzyme cannot be excluded as suggested by the higher variability of
568 amide I/amide II ratio in PMIRRAS measurements, and further revealed by the lower
569 thickness obtained by ellipsometry, which suggested some flattening of the enzyme.

570 The stability of the 6-MHA-SAM/Mv BOD bioelectrodes apparently differs from the previous
571 measurements that we made on SPR chips at pH 6¹⁶, where we observed a decrease of more
572 than 30% of the catalytic signal during similar duration. The only difference between the two
573 experiments is that in the current work we are continuously cycling the electrode potential,
574 while in the previous one, we made one cycle every 1000 s and held the electrode at OCP the
575 rest of the time. We used this protocol in the present work, and observed a decrease of the
576 catalytic current of 50%, 15%, 25% and 28%, respectively at pH 3.6, 4.6, 6 and 7.5 (Figure
577 6B). We undertook comparative chronoamperometry experiments with 6-MHA-SAM
578 modified by Mv BOD adsorbed at pH 6 at two different potentials: one situated on the plateau
579 for catalytic O₂ reduction, i.e. + 0.13 V vs Ag/AgCl, and the other close to the OCP, i.e. +
580 0.53 V vs Ag/AgCl. 4 different pHs (i.e. pH 4.6, 5.5, 6 and 6.5) above and below the pKa of

581 the SAM, and in which the enzyme activity is high and comparable, were studied. In the pH
582 range investigated, the electrostatic interactions between Mv BOD and the SAM are either
583 weak or repulsive. Typical curves are provided for the bioelectrodes transferred to pH 4.6
584 (Figure 6D) or pH 6 (Figure 6E).

585 A first observation is that the catalytic signals are more stable at pH 4.6, a condition where
586 both the SAM and the enzyme are neutral. The second main conclusion is that the activity loss
587 is much lower at the lowest applied potential (Table S3). The zero charge potential of the 6-
588 MHA-SAM reported in the literature is $E_{pzc} = + 0.116$ V vs Ag/AgCl, thus a value close to the
589 lower applied potential in this work, and much lower than OCP⁴⁴. This implies that when
590 applying a potential of + 0.53 V, the electrode surface charge is high and induces a strong
591 electric field. Taken together, this underlines that strong electrostatic interactions destabilizes
592 the Mv BOD bioelectrode.

593

594 **CONCLUSION**

595 The practical use of devices such as biosensors, bioreactors or biofuel cells based on redox
596 enzyme activity, relies on the controlled, efficient and stable immobilization of the protein on
597 solid conductive supports. The results obtained in this work provide key parameters to
598 propose new solutions to improve the process. Thanks to a multidisciplinary approach
599 coupling electrochemistry to SPR, ellipsometry and PMIRRAS, we have demonstrated the
600 correlation between enzyme loading, conformation and catalytic activity. The results have
601 been rationalized according to an electrostatic model, where the global charge of the protein
602 influences the rate of adsorption, while the enzyme dipole moment and the charge in the
603 vicinity of the CuT1, the entry site of electrons, influences the enzyme orientation, then the
604 electron transfer rate. We have also demonstrated that strong electrostatic field on the
605 electrode boundary at potentials far from zero-point charge deteriorates enzyme stability.

606 Whether this is a general rule for enzymes on electrochemical interfaces, and whether this
607 could induce changes in the enzyme conformation should be an interesting matter of future
608 discussion.

609 One objective of this work was to evaluate to which extent the hypothesis and main
610 conclusions made on planar surfaces can be extended to porous carbon nanotube networks ¹⁵,
611 ⁴⁵. Actually, Mazurenko et al. studied the consequences of BOD adsorption on carbon
612 nanotubes presenting different surface chemistry on the electrocatalytic activity. The
613 experiments conducted in the current work show that the main parameters for enzyme
614 orientation for direct electrical wiring which are determined on planar electrodes are
615 conserved on carbon nanotube networks. That means that rationalization of other enzyme-
616 based bioelectrodes should be gained by the examination of enzyme behavior on planar
617 electrodes taking mainly into account dipole moments, both the direction and value, and the
618 environment of the entry/exit site of electrons on the protein. However, we have also
619 highlighted in this work the dynamics of the protein on SAM-gold electrodes upon changes in
620 the local pH environment which affects the efficiency of the catalysis. Even if immobilization
621 on a porous material with multiple points of contact should restrict protein mobility, our
622 results provide one explanation of the low efficiency of redox proteins in most biodevices.
623 Local variation of pH occurs in the course of electrocatalysis, and the effect on enzyme
624 conformation, stability or orientation in the immobilized state require in-depth investigations,
625 using combination of techniques ⁴⁶⁻⁴⁷. This will open avenues towards new material and
626 architecture design to protect enzymes against local pH variation.

627

628 **SUPPORTING INFORMATION CONTENT**

629 CV catalytic signal as a function of sweep rate (Figure S1); pKa determination of 6-MHA-SAM
630 (Figure S2); SPR angle variation as a function of pH (Figure S3); homogeneous activity at RT or 4°C

631 as a function of pH (Figure S4); temperature and pH dependency of Mv BOD aggregation (Figure S5);
632 Control experiments using unfolded and denaturated BOD (Figures S6 and S7); electrochemical
633 behavior of ABTS and Mickaelis constant determination (Figure S8); Electrocatalysis on 11-MUA
634 (Figure S9) ant butanethiol (BT) (Figure S10, Table S1); Control experiments on 6-MHA-SAMs
635 (Figure S11); Effect of Mv BOD concentration on the electrocatalytic activity (Figure S12 and Table
636 S2); electroactivity loss with time as a function of applied potential at different pH (Table S3). This
637 information is available free of charge on the ACS Publication website.

638 **AUTHOR CONTRIBUTION**

639 **Corresponding Author**

640 *e-mail for E.L.: lojou@imm.cnrs.fr

641 V.P.H. has done the electrochemistry, homogeneous enzyme activity measurements and
642 ellipsometry experiments, and contributed to the redaction of the manuscript. I.M. initiated
643 the modeling of the electrochemical curves. R.C. was in charge of protein purification, and
644 protein modeling. M.T. made the PMIRRAS experiments, and S.C. and S.L. made the
645 PMIRRAS analysis. D.D. made the ellipsometry analysis. M.I. realized the aggregation
646 experiments and analysis of the data. I.M., M.I. and A.P. participated to the discussion of the
647 results. E.L is the initiator and director of the project and participated in all steps.

648 **Competing financial interests**

649 The authors declare no competing financial interests.

650

651 **ACKNOWLEDGMENT**

652 This work was supported by ANR (ENZYMOR-ANR-16-CE05- 0024), Région PACA
653 (Optolen Project) and Aix-Marseille University for V. Hitaishi's funding. The authors want to
654 thank L. Zuily (BIP, CNRS Marseille) for technical support in protein aggregation
655 characterization. They would like to thank Dr M. Guiral and Dr M.T. Giudici-Ortoni (BIP-
656 CNRS, Marseille) for fruitful discussion, and Y. Malier, J-J. Simon and L. Escoubas for their

657 useful advises and expertise on the field of ellipsometry. Amano Company is also thanked for
658 the kind gift of BOD.

659

660 REFERENCES

- 661 1. Kulkarni, A.; Siahrostami, S.; Patel, A.; Norskov, J. K., Understanding Catalytic
662 Activity Trends in the Oxygen Reduction Reaction. *Chemical Reviews* **2018**, 118, 2302-2312.
- 663 2. Xiong, Y.; Yang, Y.; DiSalvo, F. J.; Abruna, H. D., Pt-Decorated Composition-
664 Tunable Pd-Fe@Pd/C Core-Shell Nanoparticles with Enhanced Electrocatalytic Activity
665 toward the Oxygen Reduction Reaction. *Journal of the American Chemical Society* **2018**, 140,
666 7248-7255.
- 667 3. Holewinski, A.; Idrobo, J. C.; Lincic, S., High-performance Ag-Co alloy catalysts for
668 electrochemical oxygen reduction. *Nature Chemistry* **2014**, 6, 828-834.
- 669 4. Mukherjee, S.; Mukherjee, A.; Bhagi-Damodaran, A.; Mukherjee, M.; Lu, Y.; Dey,
670 A., A biosynthetic model of cytochrome c oxidase as an electrocatalyst for oxygen reduction.
671 *Nature Communications* **2015**, 6, 8467.
- 672 5. Mano, N.; de Poulpiquet, A., O₂ Reduction in Enzymatic Biofuel Cells. *Chemical*
673 *reviews* **2017**, 118, 2392-2468.
- 674 6. Mazurenko, I.; Wang, X.; de Poulpiquet, A.; Lojou, E., H₂/O₂ enzymatic fuel cells:
675 from proof-of-concept to powerful devices. *Sustainable Energy & Fuels* **2017**, 1, 1475-1501.
- 676 7. de Poulpiquet, A.; Kjaergaard, C. H.; Rouhana, J.; Mazurenko, I.; Infossi, P.; Gounel,
677 S.; Gadiou, R.; Giudici-Ortoni, M. T.; Solomon, E. I.; Mano, N.; Lojou, E., Mechanism of
678 Chloride Inhibition of Bilirubin Oxidases and Its Dependence on Potential and pH. *ACS*
679 *Catalysis* **2017**, 7, 3916-3923.
- 680 8. de Poulpiquet, A.; Marques-Knopf, H.; Wernert, V.; Giudici-Ortoni, M. T.; Gadiou,
681 R.; Lojou, E., Carbon nanofiber mesoporous films: efficient platforms for bio-hydrogen
682 oxidation in biofuel cells. *Physical Chemistry Chemical Physics* **2014**, 16, 1366-1378.
- 683 9. Mazurenko, I.; de Poulpiquet, A.; Lojou, E., Recent developments in high surface area
684 bioelectrodes for enzymatic fuel cells. *Current Opinion in Electrochemistry* **2017**, 5, 74-84.
- 685 10. Sakai, K.; Xia, H.; Kitazumi, Y.; Shirai, O.; Kano, K., Assembly of direct-electron-
686 transfer-type bioelectrodes with high performance. *Electrochimica Acta* **2018**, 271, 305-311.
- 687 11. Lisdat, F., Trends in the layer-by-layer assembly of redox proteins and enzymes in
688 bioelectrochemistry. *Current Opinion in Electrochemistry* **2017**, 5, 165-172.
- 689 12. Mazurenko, I.; Monsalve, K.; Infossi, P.; Giudici-Ortoni, M. T.; Topin, F.; Mano,
690 N.; Lojou, E., Impact of substrate diffusion and enzyme distribution in 3D-porous electrodes:
691 a combined electrochemical and modelling study of a thermostable H₂/O₂ enzymatic fuel cell.
692 *Energy & Environmental Science* **2017**, 10, 1966-1982.
- 693 13. Al-Lolage, F. A.; Meneghello, M.; Ma, S.; Ludwig, R.; Bartlett, P. N., A flexible
694 method for the stable, covalent immobilization of enzymes at electrode surfaces.
695 *ChemElectroChem* **2017**, 4, 1528-1534.
- 696 14. Hitaishi, V. P.; Clement, R.; Bourassin, N.; Baaden, M.; de Poulpiquet, A.; Sacquin-
697 Mora, S.; Ciaccafava, A.; Lojou, E., Controlling Redox Enzyme Orientation at Planar
698 Electrodes. *Catalysts* **2018**, 8, 192.
- 699 15. Mazurenko, I.; Monsalve, K.; Rouhana, J.; Parent, P.; Laffon, C.; Goff, A. L.;
700 Szunerits, S.; Boukherroub, R.; Giudici-Ortoni, M.-T. r. s.; Mano, N., How the intricate

701 interactions between carbon nanotubes and two bilirubin oxidases control direct and mediated
702 O₂ reduction. *ACS applied materials & interfaces* **2016**, 8, 23074-23085.

703 16. Gutierrez-Sanchez, C.; Ciaccafava, A.; Blanchard, P. Y.; Monsalve, K.; Giudici-
704 Ortoni, M. T.; Lecomte, S.; Lojou, E., Efficiency of Enzymatic O₂ Reduction by
705 *Myrothecium verrucaria* Bilirubin Oxidase Probed by Surface Plasmon Resonance,
706 PMIRRAS, and Electrochemistry. *ACS Catalysis* **2016**, 6, 5482-5492.

707 17. Gentil, S.; Carriere, M.; Cosnier, S.; Gounel, S.; Mano, N.; Le Goff, A., Direct
708 Electrochemistry of Bilirubin Oxidase from *Magnaporthe oryzae* on Covalently-
709 Functionalized MWCNT for the Design of High-Performance Oxygen-Reducing Biocathodes.
710 *Chemistry-a European Journal* **2018**, 24, 8404-8408.

711 18. Blout, A.; Billon, F.; Calers, C.; Methivier, C.; Pailleret, A.; Perrot, H.; Jolival, C.,
712 Orientation of a *Trametes versicolor* laccase on amorphous carbon nitride coated graphite
713 electrodes for improved electroreduction of dioxygen to water. *Electrochimica Acta* **2018**,
714 277, 255-267.

715 19. Hoarau, M.; Badiéyan, S.; Marsh, E. N. G., Immobilized enzymes: understanding
716 enzyme - surface interactions at the molecular level. *Organic & Biomolecular Chemistry*
717 **2017**, 15, 9539-9551.

718 20. Rodrigues, R. C.; Ortiz, C.; Berenguer-Murcia, A.; Torres, R.; Fernandez-Lafuente,
719 R., Modifying enzyme activity and selectivity by immobilization. *Chemical Society Reviews*
720 **2013**, 42, 6290-6307.

721 21. Chumillas, S.; Maestro, B.; Feliu, J. M.; Climent, V., Comprehensive Study of the
722 Enzymatic Catalysis of the Electrochemical Oxygen Reduction Reaction (ORR) by
723 Immobilized Copper Efflux Oxidase (CueO) From *Escherichia coli*. *Frontiers in Chemistry*
724 **2018**, 6, 358.

725 22. Yang, S. J.; Liu, J.; Quan, X. B.; Zhou, J., Bilirubin Oxidase Adsorption onto Charged
726 Self-Assembled Monolayers: Insights from Multiscale Simulations. *Langmuir* **2018**, 34,
727 9818-9828.

728 23. Harris, T.; Heidary, N.; Kozuch, J.; Frielingsdorf, S.; Lenz, O.; Mroginski, M. A.;
729 Hildebrandt, P.; Zebger, I.; Fischer, A., In Situ Spectroelectrochemical Studies into the
730 Formation and Stability of Robust Diazonium-Derived Interfaces on Gold Electrodes for the
731 Immobilization of an Oxygen-Tolerant Hydrogenase. *Acs Applied Materials & Interfaces*
732 **2018**, 10, 23380-23391.

733 24. Krzeminski, L.; Cronin, S.; Ndamba, L.; Canters, G. W.; Aartsma, T. J.; Evans, S. D.;
734 Jeuken, L. J. C., Orientational Control over Nitrite Reductase on Modified Gold Electrode and
735 Its Effects on the Interfacial Electron Transfer. *Journal of Physical Chemistry B* **2011**, 115,
736 12607-12614.

737 25. Climent, V.; Fu, Y. C.; Chumillas, S.; Maestro, B.; Li, J. F.; Kuzume, A.; Keller, S.;
738 Wandlowski, T., Probing the Electrocatalytic Oxygen Reduction Reaction Reactivity of
739 Immobilized Multicopper Oxidase CueO. *Journal of Physical Chemistry C* **2014**, 118, 15754-
740 15765.

741 26. Jin, B.; Wang, G.-X.; Millo, D.; Hildebrandt, P.; Xia, X.-H., Electric-field control of
742 the pH-dependent redox process of cytochrome c immobilized on a gold electrode. *The*
743 *Journal of Physical Chemistry C* **2012**, 116, 13038-13044.

744 27. Hexter, S. V.; Esterle, T. F.; Armstrong, F. A., A unified model for surface
745 electrocatalysis based on observations with enzymes. *Physical Chemistry Chemical Physics*
746 **2014**, 16, 11822-11833.

747 28. Rakic, A. D.; Djuricic, A. B.; Elazar, J. M.; Majewski, M. L., Optical properties of
748 metallic films for vertical-cavity optoelectronic devices. *Applied Optics* **1998**, 37, 5271-5283.

749 29. Voros, J., The density and refractive index of adsorbing protein layers. *Biophysical*
750 *Journal* **2004**, 87, 553-561.

- 751 30. Utesch, T.; Millo, D.; Castro, M. A.; Hildebrandt, P.; Zebger, I.; Mroginski, M. A.,
752 Effect of the protonation degree of a self-assembled monolayer on the immobilization
753 dynamics of a [NiFe] hydrogenase. *Langmuir* **2013**, *29*, 673-682.
- 754 31. Felder, C. E.; Prilusky, J.; Silman, I.; Sussman, J. L., A server and database for dipole
755 moments of proteins. *Nucleic acids research* **2007**, *35*, W512-W521.
- 756 32. Dolinsky, T. J.; Nielsen, J. E.; McCammon, J. A.; Baker, N. A., PDB2PQR: an
757 automated pipeline for the setup of Poisson-Boltzmann electrostatics calculations. *Nucleic*
758 *Acids Research* **2004**, *32*, W665-W667.
- 759 33. Marmisollé, W. A.; Capdevila, D. A.; de la Llave, E.; Williams, F. J.; Murgida, D. H.,
760 Self-Assembled Monolayers of NH₂-Terminated Thiolates: Order, pKa, and Specific
761 Adsorption. *Langmuir* **2013**, *29*, 5351-5359.
- 762 34. Bryant, M. A.; Crooks, R. M., Determination of surface pKa values of surface-
763 confined molecules derivatized with pH-sensitive pendant groups. *Langmuir* **1993**, *9*, 385-
764 387.
- 765 35. Pankratov, D.; Sotres, J.; Barrantes, A.; Arnebrant, T.; Shleev, S., Interfacial behavior
766 and activity of laccase and bilirubin oxidase on bare gold surfaces. *Langmuir* **2014**, *30*, 2943-
767 2951.
- 768 36. McArdle, T.; McNamara, T. P.; Fei, F.; Singh, K.; Blanford, C. F., Optimizing the
769 Mass-Specific Activity of Bilirubin Oxidase Adlayers through Combined Electrochemical
770 Quartz Crystal Microbalance and Dual Polarization Interferometry Analyses. *Acs Applied*
771 *Materials & Interfaces* **2015**, *7*, 25270-25280.
- 772 37. Tapley, T. L.; Korner, J. L.; Barge, M. T.; Hupfeld, J.; Schauerte, J. A.; Gafni, A.;
773 Jakob, U.; Bardwell, J. C. A., Structural plasticity of an acid-activated chaperone allows
774 promiscuous substrate binding. *Proceedings of the National Academy of Sciences of the*
775 *United States of America* **2009**, *106*, 5557-5562.
- 776 38. Yamaguchi, H.; Kiyota, Y.; Miyazaki, M., Techniques for Preparation of Cross-
777 Linked Enzyme Aggregates and Their Applications in Bioconversions. *Catalysts* **2018**, *8*,
778 174.
- 779 39. Otsuka, K.; Sugihara, T.; Tsujino, Y.; Osakai, T.; Tamiya, E., Electrochemical
780 consideration on the optimum pH of bilirubin oxidase. *Analytical Biochemistry* **2007**, *370*, 98-
781 106.
- 782 40. Smalley, J. F.; Feldberg, S. W.; Chidsey, C. E.; Linford, M. R.; Newton, M. D.; Liu,
783 Y.-P., The kinetics of electron transfer through ferrocene-terminated alkanethiol monolayers
784 on gold. *The Journal of Physical Chemistry* **1995**, *99*, 13141-13149.
- 785 41. Singh, K.; McArdle, T.; Sullivan, P. R.; Blanford, C. F., Sources of activity loss in the
786 fuel cell enzyme bilirubin oxidase. *Energy & Environmental Science* **2013**, *6*, 2460-2464.
- 787 42. Dagys, M.; Laurynėnas, A.; Ratautas, D.; Kulys, J.; Vidžiūnaitė, R.; Talaikis, M.;
788 Niaura, G.; Marcinkevičienė, L.; Meškys, R.; Shleev, S., Oxygen electroreduction catalysed
789 by laccase wired to gold nanoparticles via the trinuclear copper cluster. *Energy &*
790 *Environmental Science* **2017**, *10*, 498-502.
- 791 43. Sugimoto, Y.; Kitazumi, Y.; Tsujimura, S.; Shirai, O.; Yamamoto, M.; Kano, K.,
792 Electrostatic interaction between an enzyme and electrodes in the electric double layer
793 examined in a view of direct electron transfer-type bioelectrocatalysis. *Biosensors and*
794 *Bioelectronics* **2015**, *63*, 138-144.
- 795 44. Smalley, J. F., Potential of Zero Charge and Its Temperature Derivative for Au(111)
796 Electrode vertical bar Alkanethiol SAM1.0 M Aqueous Electrolyte Solution Interfaces:
797 Impact of Electrolyte Solution Ionic Strength and Its Effect on the Structure of the Modified
798 Electrode/Electrolyte Solution Interface. *J. Phys. Chem. C* **2017**, *121*, 9260-9272.
- 799 45. Hoshikawa, Y.; Castro-Muniz, A.; Tawata, H.; Nozaki, K.; Yamane, S.; Itoh, T.;
800 Kyotani, T., Orientation Control of Trametes Laccases on a Carbon Electrode Surface to

801 Understand the Orientation Effect on the Electrocatalytic Activity. *Bioconjugate Chemistry*
802 **2018**, 29, 2927-2935.

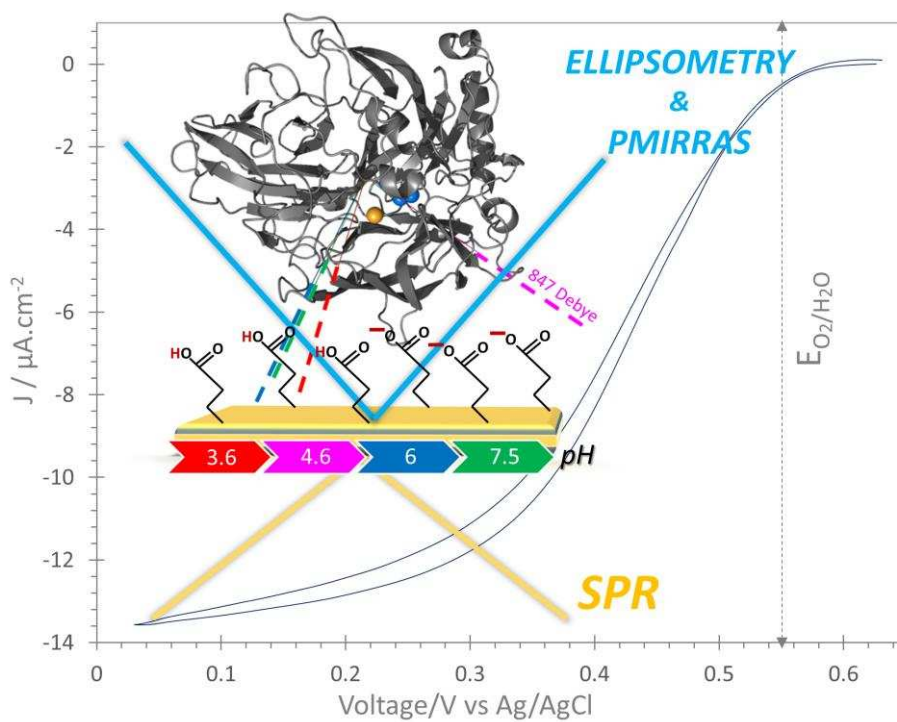
803 46. Zhang, Y. F.; Tsitkov, S.; Hess, H., Proximity does not contribute to activity
804 enhancement in the glucose oxidase-horseradish peroxidase cascade. *Nature Communications*
805 **2016**, 7, 13982.

806 47. Lancaster, L.; Abdallah, W.; Banta, S.; Wheeldon, I., Engineering enzyme
807 microenvironments for enhanced biocatalysis. *Chemical Society reviews* **2018**, 47, 5177-5186.

808

809

810 **GRAPHICAL ABSTRACT**



811